Supplementary Materials

Supplementary Table 1. Impact of Dataset Split on Observed Outcomes

	Schaefer 200 Nodes			Schaefer 300 Nodes		
	Sample 1	Sample 2	Consensus between samples	Sample 1	Sample 2	Consensus between samples
Static FC						
Q-metric	0.97	0.96	0.93	0.94	0.94	0.88
Number of Partitions	0.95	0.93	0.88	0.99	0.99	0.98
Time-Varying FC						
Mean Q-metric	0.90	0.92	0.83	0.89	0.88	0.77
Standard Deviation of the Q-metric	0.88	0.88	0.76	0.83	0.83	0.66

Data are shown as a fraction of times that a dataset split (out of a total of 500 random splits) was consistent with results obtained in the original split. Consensus between samples is the fraction of times results from both samples in a single split were consistent with the original split. FC: Functional Connectivity

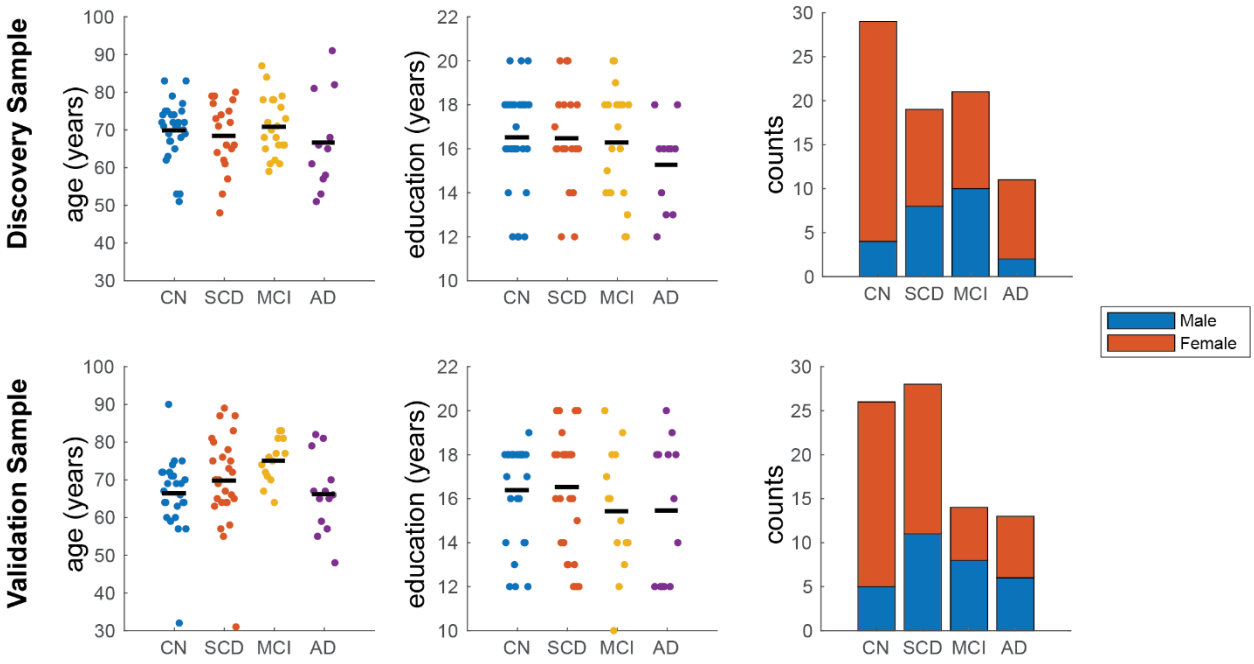

Supplementary Figure 1. A detailed overview of key demographic variables for the Discovery (Top) and Validation (Bottom) samples. Individual points in scatter plots represent individual subjects while the mean is denoted by the black line. CN: Cognitively Normal; SCD: Subjective Cognitive Decline; MCI: Mild Cognitive Impairment; AD: Alzheimer's Disease

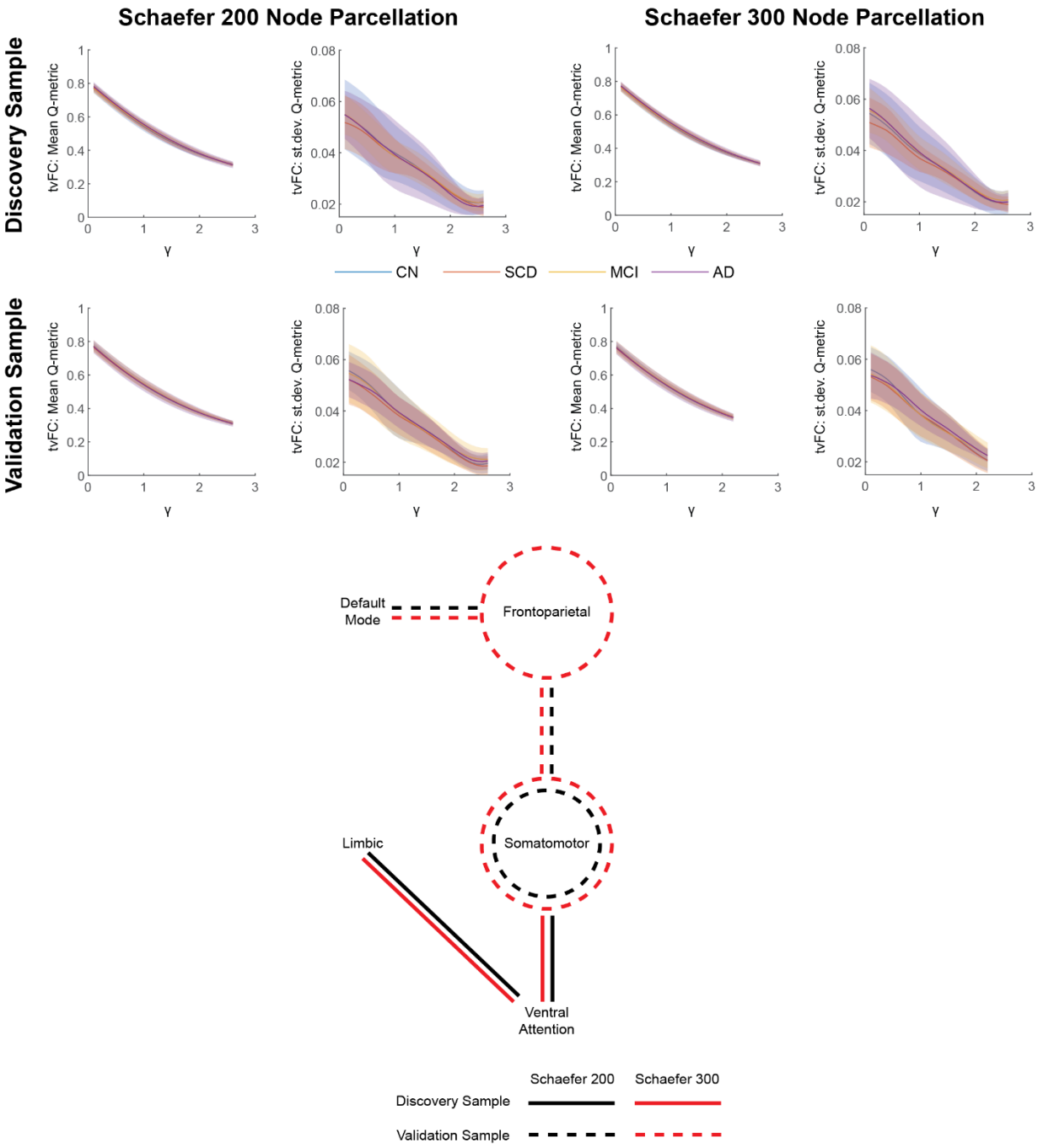

Supplementary Figure 2. Modularity outcomes for time-varying functional connectivity (tvFC) with a 95-time point (~111 second) window (Top) and temporal stability differences at $p<0.05$ uncorrected. These results, with a longer window, are largely consistent with the ~1-minute window results reported in the main text. CN: Cognitively Normal; SCD: Subjective Cognitive Decline; MCI: Mild Cognitive Impairment; AD: Alzheimer's Disease

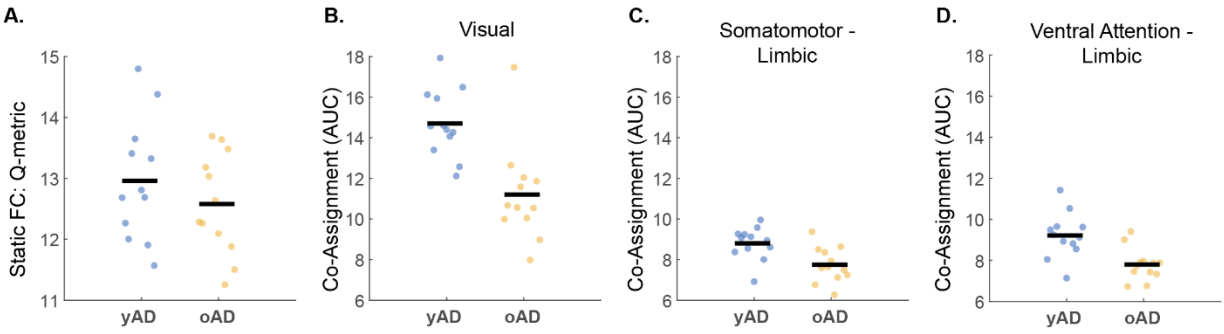

Supplementary Figure 3. Differences in modularity outcomes in younger (yAD) compared to older Alzheimer's disease (oAD) participants for the Schaefer 200 node parcellation. (A) Area under the curve (AUC) of the modularity Q-metric for conventional (static) functional connectivity. (B-D) Time-varying functional connectivity stability (Co-Assignment AUC) for visual (B), somatomotor-limbic interaction (C), and ventral attention-limbic interaction resting-state network blocks.

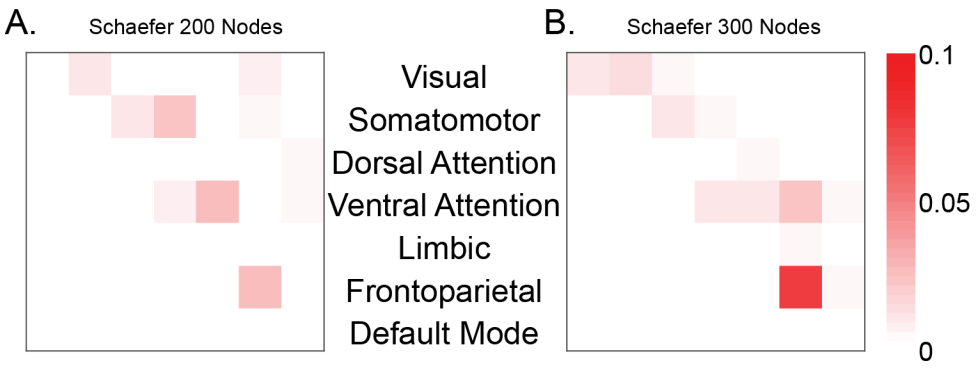

Supplementary Figure 4. Robustness of network block temporal stability (Co-Assignment across windows) of the original dataset split, compared to 500 additional random dataset splits, for the (A) 200 node and (B) 300 node parcellations. Rows and columns are labeled according to the canonical resting-state networks. Data are shown as the fraction of times (out of 500) a significant group difference was observed (p<0.05, uncorrected) for both samples in a split.

Supplementary Methods

Image Processing

Overview. The image processing pipeline was developed at Indiana University School of Medicine, following best practices guidelines in the neuroimaging field (Satterthwaite et al., 2013, Power et al., 2015, Parkes et al., 2018, Lindquist et al., 2019). It is a Matlab-based set of scripts, which utilize FSL (Jenkinson et al., 2012), AFNI (Cox, 1996), and ANTS (http://stnava.github.io/ANTs/) to take data from raw neuroimaging format to connectivity matrices, while maintaining the data in native participant space. The following sections describe each preprocessing section in detail with supporting references.

T1 preprocessing

Dicom Import: Data are first converted from raw dicom (.dcm) format to nifti (.nii) with the dcm2niiX tool (Li et al., 2016)(https://github.com/rordenlab/dcm2niix).

Denoising: For each dataset, the T1 nifti image is then denoised using an optimized nonlocal means filter for 3D MRI implemented in Matlab (Coupé et al., 2010, Coupé et al., 2008), to improve subsequent brain extraction, tissue segmentation, and registration steps.

Bias Field Correction: Bias field correction is done within the FSL's FAST tool (Zhang et al., 2001) with *robustfov* field-of-view cropping.

Brain Extraction: Across the whole sample, first pass brain extraction was carried out with ANTS (https://github.com/ANTsX/ANTs) using an openly available OASIS data template (https://figshare.com/articles/ANTs_ANTsR_Brain_Templates/915436). All brain masks were then visually checked for quality in Matlab by visualizing 5 evenly spaced slices of the T1 with the mask as a semi-transparent overlay. For any participant with a poor quality mask, brain extraction was repeated with an alternative template from the same source that was derived from the Nathan Kline Institute (http://dx.doi.org/10.15387/fcp_indi.corr.nki1). For any remaining participants for which a suitable brain mask was still not attained, FSL bet with -B option was used to derive a mask, by tuning the fractional intensity and vertical gradient in fractional intensity parameters independently for each participant to obtain a suitable mask. Finally, any gaps/holes in the mask were filled with *fslmaths -fillh* option and a final brain masked image was extracted.

Standard Space Registration: In order to apply parcellations in native space, linear and nonlinear transformations were generated for each participant T1 to/from Montreal Neurological Institute (MNI) standard space via the following:

1. FSL FLIRT (Jenkinson and Smith, 2001) linear 6 degrees of freedom registration (dof6) to MNI.
2. FSL FLIRT affine 12 degrees of freedom registration (dof12) of dof6 to MNI.
3. FSL FNIRT (Andersson et al., 2010) nonlinear warp of dof12 to MNI

The 2 transformation matrices and warp field were then inverted with the *convert_xfm* and *invwarp* FSL utilities, respectively. Quality of spatial transformations was visually assessed by overlay of the contour of standard space participant T1 onto the MNI152 template.

Tissue-Type Segmentation: Tissue-probability maps (gray matter (GM), white matter (WM), and cerebrospinal fluid (CSF)) and a tissue-type segmentation were generated with FSL FAST. Additionally, a subcortical segmentation/mask was generated with FIRST (Patenaude et al., 2011). The following steps then utilized *fslmaths* to 'clean-up' the segmentation and generate images necessary for subsequent preprocessing:

1. Erroneous CSF voxels were removed from the subcortical mask by removing those voxels that were present in the CSF mask.
2. The 'cleaned-up' subcortical mask added into the tissue-type segmentation as GM.
3. A single erosion was performed on GM and CSF masks.
4. An eroded WM mask was generated by eroding WM mask 3 times.
5. An MNI template dilated CSF ventricle mask was transformed into participant space and intersected with the eroded CSF mask to create a participant-specific eroded CSF ventricle mask. [Masks generated in steps 3-5 were used in fMRI Nuisance Regression]
6. The WM/CSF boundaries of the ventricles (which often get erroneously segmented as GM) were removed from the GM mask via the following:
    a. An interface of WM/CSF was generated as the overlap of the dilated versions of the two masks.
    b. The interface was then masked by the dilated template CSF mask from (5) to isolate the interface around the ventricles.
    c. FSL's *cluster* tool was then used to take the largest contiguous element of that mask (the area around the ventricles), thus removing any residual small clusters that may not have been caught by the masking in (b).
    d. Finally, the inverse of the WM/CSF ventricle mask was applied to the GM mask to remove any GM misclassified voxels at the WM/CSF boundary.

Registering Parcellations into Native Space: Cortical brain parcellations were registered into participant native space via the transformations generated in [*Standard Space Registration*] section. These images were then masked by the participant's GM mask. Further, to ensure complete coverage of participants' GM by parcellation an iterative procedure of dilation followed by GM re-masking was carried out 3 times. The cortical GM parcellations were then masked by the inverses of the dilated subcortical mask and the native space-generated cerebellar mask (generated with FSL FIRST) to remove any erroneously assigned voxels that may have resulted from the spatial transformations or iterative dilation/re-masking procedure. The final GM parcellations were then dilated once (to be used in fMRI preprocessing).

fMRI preprocessing

Dicom import: See [T1 preprocessing: Dicom Import].

Distortion Correction: FSL's *topup* and was used for correction of susceptibility induced distortions, by utilizing 3 pairs of opposite phase-encoding (AP-PA) spin-eco field maps to estimate a susceptibility-induced off-resonance field (Andersson et al., 2003) that was used to correct the fMRI data via *applytopup.*

Motion Correction: FSL's mcFLIRT was used to correct for motion via affine registration to the mean volume (Jenkinson et al., 2002).

Registration of T1 to fMRI: A mean volume was created from the motion corrected data and nonbrain tissue was removed via FSL *bet* -R. The following steps describe the stepwise registration of each participant's T1 to his/her brain-extracted mean fMRI volume:

1. FSL FLIRT linear 6 degrees of freedom registration of T1 to mean fMRI.
2. Apply transformation from (1) to the WM mask.
3. The fMRI mean is then registered to the T1 and WM mask from (1) and (2) with FLIRT boundary-based registration cost function.
4. The transformations from (1) and (3) are then concatenated to produce a single affine transformation from native T1 to native fMRI.

Registration of Other Images: The transformation generated in the previous step is then used to register the following onto fMRI native space: brain mask, tissue-type masks, and parcellations.

Intensity Normalization: fMRI data were normalized to a global 4D mean of 1000 using *fslmaths -ing* option.

Nuisance Regression: For these data a 3-step nuisance regression procedure was utilized. First, the Independent Component Analysis-Automatic Removal of Motion Artifacts (ICA_AROMA) (Pruim et al., 2015) was used to regress out motion related signal while preserving the temporal degrees of freedom in the data, which is necessary for the time-varying analyses employed. Second, the anatomical component-based noise correction method (aCompCor) (Behzadi et al., 2007) was implemented in Matlab and was used to regress out the first 5 principal components of WM and of ventricular CSF signal obtained from the fMRI space-eroded masks. Finally, global signal was regressed from the fMRI data.

Demean and Detrend: Each voxel across time was mean-centered and a linear trend was removed with the Matlab *detrend* function.

Bandpass Filtering: A first order Butterworth filter (0.009 – 0.08 Hz) was applied to the data via the Matlab butter and filtfilt functions.

Parcellation timeseries: The final fMRI voxel time courses were then averaged for each region of interest (ROI) in the parcellation, to obtain the timeseries that were used to generate static and time-varying functional connectivity matrices.

References

ANDERSSON, J. L. R., JENKINSON, M. & SMITH, S. 2010. Non-linear registration, aka spatial normalization. *FMRIB technical report TR07JA2*.

ANDERSSON, J. L. R., SKARE, S. & ASHBURNER, J. 2003. How to correct susceptibility distortions in spin-echo echo-planar images: application to diffusion tensor imaging. *NeuroImage,* 20**,** 870-888.

BEHZADI, Y., RESTOM, K., LIAU, J. & LIU, T. T. 2007. A component based noise correction method (CompCor) for BOLD and perfusion based fMRI. *NeuroImage,* 37**,** 90-101.

COUPÉ, P., MANJÓN, J. V., GEDAMU, E., ARNOLD, D., ROBLES, M. & COLLINS, D. L. 2010. Robust Rician noise estimation for MR images. *Medical Image Analysis,* 14**,** 483-493.

COUPÉ, P., YGER, P., PRIMA, S., HELLIER, P., KERVRANN, C. & BARILLOT, C. 2008. An Optimized Blockwise Nonlocal Means Denoising Filter for 3-D Magnetic Resonance Images. *Medical Imaging, IEEE Transactions on,* 27**,** 425-441.

COX, R. W. 1996. AFNI: Software for Analysis and Visualization of Functional Magnetic Resonance Neuroimages. *Computers and Biomedical Research,* 29**,** 162-173.

JENKINSON, M., BANNISTER, P., BRADY, M. & SMITH, S. 2002. Improved Optimization for the Robust and Accurate Linear Registration and Motion Correction of Brain Images. *NeuroImage,* 17**,** 825-841.

JENKINSON, M., BECKMANN, C. F., BEHRENS, T. E. J., WOOLRICH, M. W. & SMITH, S. M. 2012. FSL. *NeuroImage,* 62**,** 782-790.

JENKINSON, M. & SMITH, S. 2001. A global optimisation method for robust affine registration of brain images. *Medical Image Analysis,* 5**,** 143-156.

LI, X., MORGAN, P. S., ASHBURNER, J., SMITH, J. & RORDEN, C. 2016. The first step for neuroimaging data analysis: DICOM to NIfTI conversion. *Journal of Neuroscience Methods,* 264**,** 47-56.

LINDQUIST, M. A., GEUTER, S., WAGER, T. D. & CAFFO, B. S. 2019. Modular preprocessing pipelines can reintroduce artifacts into fMRI data. *Human Brain Mapping,* 40**,** 2358-2376.

PARKES, L., FULCHER, B., YÜCEL, M. & FORNITO, A. 2018. An evaluation of the efficacy, reliability, and sensitivity of motion correction strategies for resting-state functional MRI. *NeuroImage,* 171**,** 415-436.

PATENAUDE, B., SMITH, S. M., KENNEDY, D. N. & JENKINSON, M. 2011. A Bayesian model of shape and appearance for subcortical brain segmentation. *NeuroImage,* 56**,** 907-922.

POWER, J. D., SCHLAGGAR, B. L. & PETERSEN, S. E. 2015. Recent progress and outstanding issues in motion correction in resting state fMRI. *NeuroImage,* 105**,** 536-551.

PRUIM, R. H. R., MENNES, M., VAN ROOIJ, D., LLERA, A., BUITELAAR, J. K. & BECKMANN, C. F. 2015. ICA-AROMA: A robust ICA-based strategy for removing motion artifacts from fMRI data. *NeuroImage,* 112**,** 267-277.

SATTERTHWAITE, T. D., ELLIOTT, M. A., GERRATY, R. T., RUPAREL, K., LOUGHEAD, J., CALKINS, M. E., EICKHOFF, S. B., HAKONARSON, H., GUR, R. C., GUR, R. E. & WOLF, D. H. 2013. An improved framework for confound regression and filtering for control of motion artifact in the preprocessing of resting-state functional connectivity data. *NeuroImage,* 64**,** 240-256.

ZHANG, Y., BRADY, M. & SMITH, S. 2001. Segmentation of brain MR images through a hidden Markov random field model and the expectation-maximization algorithm. *IEEE Transactions on Medical Imaging,* 20**,** 45-57.